Supplemental Methods and Materials:

T785 Synthesis

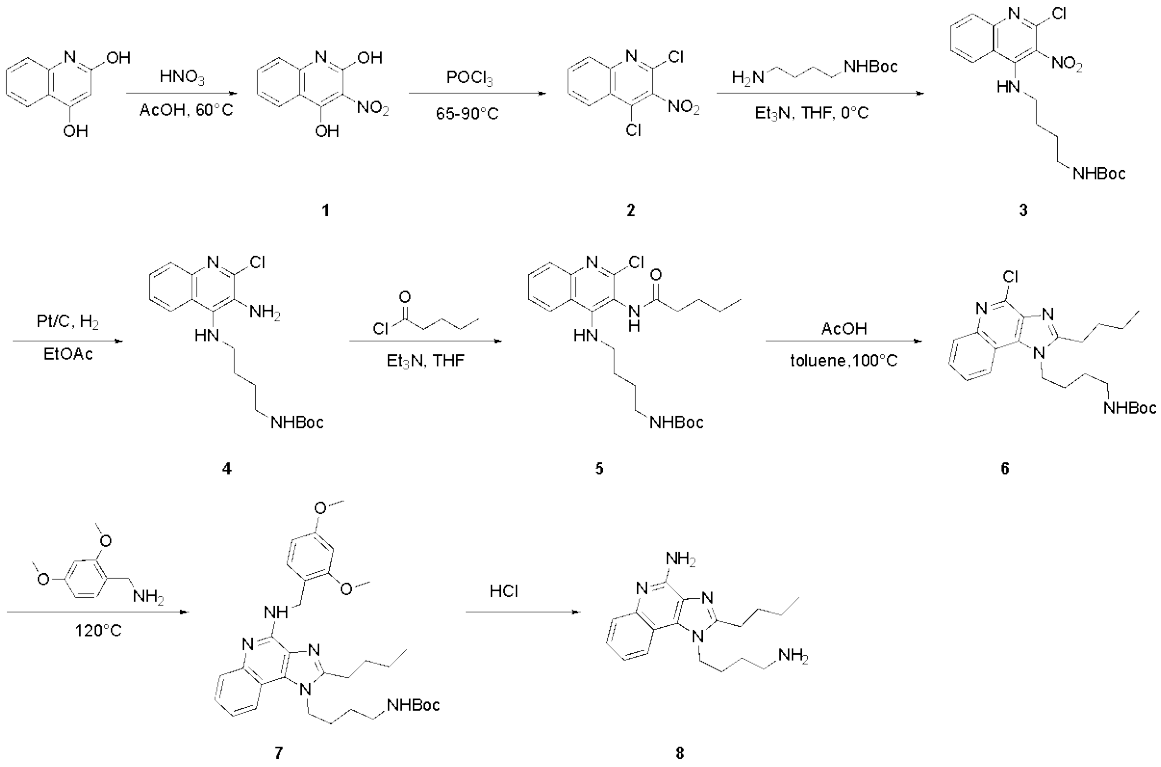

3-nitroquinoline-2,4-diol (**1**). To a solution of quinoline-2,4-diol (260 g, 1.61 mol, 1 eq) in AcOH (1.2 L) was added fuming nitric acid (152.49 g, 2.42 mol, 108.92 mL, 1.5 eq) dropwise at 0°C. The mixture was stirred at 65°C for 5 hours. LCMS showed the reactant was consumed. The mixture was cooled to 25°C and quenched by addition of ice-water (500 mL). The product was separated by filtration and washed with water (500 mL x 3), dried to give 3-nitroquinoline-2,4-diol (320 g, 1.52 mol, 94.29% yield) as yellow solid. The crude product was used in the next step without further purification. LC/MS: m/z = 207.0 $[M+H]^+$ 1H NMR (DMSO-d_6, 400 MHz) δ 11.96 (s, 1H), 8.04 (d, J = 8.0 Hz, 1H), 7.64 (t, J = 7.2 Hz, 1H), 7.34 (d, J = 8.0 Hz, 1H), 7.27 (t, J = 7.2 Hz, 1H).

2,4-dichloro-3-nitroquinoline (**2**). 3-nitroquinoline-2,4-diol (365 g, 1.77 mol, 1 eq) was added slowly to $POCl_3$ (2.44 kg, 15.93 mol, 1.48 L, 9 eq) at 65°C and further heated to 90°C for 12 h. LCMS showed the

starting material was consumed completely. The mixture was concentrated under vacuum. The residue was then poured into ice-water (3 L) and stirred for 0.5 h. The aqueous phase was filtered, washed by water (500 mL x 5) and the filter cake was collected and further purified by silica gel chromatography (Petroleum ether/Ethyl acetate=20/1, 3/1) to obtain 2,4-dichloro-3-nitro-quinoline (330 g, 1.32 mol, 74.39% yield, 97% purity) as yellow solid. LC/MS: m/z = 243.0 $[M+H]^+$ 1H NMR ($CDCl_3$, 400 MHz) δ 8.29 (d, J = 8.4 Hz, 1H), 8.13 (d, J = 8.4 Hz, 1H), 7.96 (t, J =8.4 Hz, 1H), 7.82 (t, J = 8.4 Hz, 1H).

Tert-butyl N-[4-[(2-chloro-3-nitro-4-quinolyl) amino]butyl]carbamate (**3**). To a mixture of 2,4-dichloro-3-nitro-quinoline (330 g, 1.36 mol, 1 eq) and tert-butyl N-(4-aminobutyl)carbamate (281.18 g, 1.49 mol, 1.1 eq) in THF (1.5 L) was added Et_3N (206.09 g, 2.04 mol, 283.48 mL, 1.5 eq) slowly at 0°C and stirred for 2 h. TLC (Petroleum ether: Ethyl acetate = 1:1, Rf = 0.43) showed the starting materials were consumed completely and one main spot was detected. The reaction was quenched by water (2 L) and extracted with EtOAc (800 mL x 3). The combined organic layer was washed by brine (1000 mL), dried over Na_2SO_4, filtered, and concentrated in vacuum. The crude product was washed by petroleum ether (1000 mL) and filtered to give tert-butyl N-[4-[(2-chloro-3-nitro-4-quinolyl) amino]butyl]carbamate (500 g, crude) as yellow solid. LC/MS: m/z = 395.2 $[M+H]^+$ 1H NMR ($CDCl_3$, 400 MHz) δ 8.12 (d, J = 7.2 Hz, 1H), 7.92 (d, J = 8.4 Hz, 1H), 7.75 (t, J =7.2 Hz, 1H), 7.53 (t, J = 7.6 Hz, 1H), 6.43 (s, 1H), 4.70 (s, 1H), 3.50-3.45 (m, 2H), 3.22-3.17(m, 2H), 1.80-1.75 (m, 2H), 1.67-1.61 (m, 2H), 1.44 (s, 9H).

Tert-butyl N-[4-[(3-amino-2-chloro-4-quinolyl)amino]butyl]carbamate (**4**). To a solution of tert-butyl N-[4-[(2-chloro-3-nitro-4-quinolyl)amino]butyl]carbamate (150 g, 379.89 mmol, 1 eq) in EtOAc (800 mL) was added Pt/C (40 g, 10% purity) under N_2. The suspension was degassed under vacuum and purged with H_2 several times. The mixture was stirred under H_2 (50 psi) at 25°C for 3 hours. LCMS and HPLC showed the starting material was consumed completely. The reaction mixture was filtered and the filtrate was concentrated to give tert-butyl N-[4-[(3-amino-2-chloro-4-quinolyl)amino]butyl]carbamate (110 g, crude) as off-white solid. LC/MS: m/z = 365.2 $[M+H]^+$ 1H NMR ($CDCl_3$, 400 MHz) δ 7.90 (d, J = 8.0 Hz, 1H), 7.79 (d, J = 7.6 Hz, 1H) 7.49-7.45 (m,2H), 4.59 (s, 1H), 4.15-4.10 (m, 2H), 3.29-3.26 (m, 2H), 3.18-3.16 (m, 2H), 1.70-1.60 (m, 4H), 1.45 (s, 9H).

Tert-butyl N-[4-[[2-chloro-3-(pentanoylamino)-4-quinolyl]amino]butyl] carbamate (**5**). To a mixture of tert-butyl N-[4-[(3-amino-2-chloro-4-quinolyl)amino]butyl] carbamate (500 g, 1.37 mol, 1 eq) and Et_3N (208.00 g, 2.06 mol, 286.11 mL, 1.5 eq) in THF (1000 mL) was added pentanoyl chloride (247.85 g, 2.06 mol, 249.10 mL, 1.5 eq) dropwise at 0°C. The mixture was stirred at 0°C for 1 h. LCMS showed the reaction was completed and desired product was detected. The mixture was poured into ice water (1000 mL) and stirred for 2 min. The aqueous phase was extracted with ethyl acetate (500 mL x 3). The combined organic phase was washed with brine (1000 mL), dried with anhydrous Na_2SO_4, filtered and concentrated in vacuum. The residue was purified by re-crystallization from EtOAc/petroleum ether (1/1, 800 mL) to give the pure tert-butyl N-[4-[[2-chloro-3-(pentanoylamino)-4-quinolyl]amino] butyl] carbamate (550 g, 1.16 mol, 84.92% yield, 95% purity) as light yellow solid. LC/MS: m/z = 449.3 $[M+H]^+$ 1H NMR (MeOD, 400 MHz) δ 8.14 (d, J = 8.4 Hz, 1H), 7.72 (d, J = 7.6 Hz, 1H), 7.67 (t, J = 8.0 Hz, 1H), 7.46 (t, J = 6.8 Hz, 1H), 3.56 (t, J = 7.2 Hz, 2H), 3.07 (t, J = 7.2 Hz, 2H), 2.51 (t, J = 7.6 Hz, 2H), 1.77-1.66 (m, 4H), 1.54-1.41 (m, 4H), 1.41 (s, 9H), 1.01 (t, J = 7.2 Hz, 3H).

Tert-butyl N-[4-(2-butyl-4-chloro-imidazo[4,5-c]quinolin-1-yl)butyl]carbamate (**6**). To a solution of tert-butyl N-[4-[[2-chloro-3-(pentanoylamino)-4-quinolyl]amino] butyl]carbamate (490 g, 1.09 mol, 1 eq) in toluene (1000 mL) was added AcOH (65.54 g, 1.09 mol, 62.42 mL, 1 eq) at 25°C. The mixture was stirred at 100°C for 15 hours. TLC indicated ~10% of reactant was remained, and one major new spot with lower polarity was detected. LCMS showed the desired product was detected. The mixture was concentrated. The residue was poured into ice water (1000 mL) and stirred for 5 min. The aqueous phase was extracted with ethyl acetate (500 mL x 3). The combined organic phase was washed with $NaHCO_3$.aq (500 mL) and brine (800 mL), dried with anhydrous Na_2SO_4, filtered and concentrated in vacuum. The residue was purified by re-crystallized from EtOAc/ petroleum ether (1/50, 500 mL) to give tert-butyl N-[4-(2-butyl-4-chloro-imidazo[4,5-c]quinolin-1- yl)butyl]carbamate (400 g, 928.14 mmol, 85.05% yield) as a white solid. LC/MS: m/z = 431.1 $[M+H]^+$ 1H NMR ($CDCl_3$, 400 MHz) δ 8.19 (d, J = 6.8 Hz, 1H), 8.09 (d, J = 7.6 Hz, 1H) 7.66-7.62 (m,2H), 4.61 (s, 1H), 4.54 (t, J = 7.6 Hz, 2H), 3.21-2.20 (m, 2H), 3.00

(t, J = 8.0 Hz, 2H), 1.97-1.88 (m, 4H), 1.71-1.69 (m, 2H), 1.55-1.49 (m, 2H), 1.42 (s, 9H), 1.01 (t, J = 7.2 Hz, 3H).

Tert-butyl N-[4-[2-butyl-4-[(2,4-dimethoxyphenyl)methylamino]imidazo[4,5-c]quinolin-1-yl]butyl]carbamate (**7**). Tert-butyl N-[4-(2-butyl-4-chloro-imidazo[4,5-c]quinolin-1-yl)butyl] carbamate (62 g, 143.86mmol, 1 eq) in (2,4-dimethoxyphenyl)methanamine (120.27 g, 719.31 mmol, 108.35 mL, 5 eq) was stirred at 120°C for 3 hr. LCMS showed the reaction was completed. The reaction was quenched by addition of water (200 mL), acidified by diluted hydrochloride acid and extracted with EtOAc (300 mL x 3). The combined organic layers were washed by brine (500 mL), dried over Na_2SO_4, filtered and concentrated under reduced pressure. The residue was purified by re-crystallization from EtOAc (200mL) to give tert-butyl N-[4-[2-butyl-4-[(2,4-dimethoxyphenyl)methylamino]imidazo[4,5-c]quinolin-1-yl]butyl]carba mate (70 g, 118.39 mmol, 82.29% yield, 95% purity) as white solid. LC/MS: m/z = 562.4 $[M+H]^+$ 1H NMR (MeOD, 400 MHz) δ 8.22 (d, J = 8.4 Hz, 1H), 8.05 (s, 1H), 7.74 (t, J = 7.6 Hz, 1H),7.66 (t, J = 8.4 Hz, 1H), 7.31 (d, J = 8.4 Hz, 1H), 6.63-6.58 (m, 1H), 6.54 (d, J = 8.0 Hz, 1H) 4.62 (t, J = 7.2 Hz, 2H), 3.82 (s, 3H), 3.79 (s, 3H), 3.12 (t, J = 6.8 Hz, 2H), 3.00 (t, J = 7.6 Hz, 2H), 1.98-1.86 (m, 4H), 1.69-1.65 (m, 2H), 1.53-1.50 (m, 2H), 1.37 (s, 9H), 1.01 (t, J = 7.6 Hz,

1-(4-aminobutyl)-2-butyl-imidazo[4,5-c]quinolin-4-amine (**9**). Tert-butyl N-[4-[2-butyl-4-[(2,4-dimethoxyphenyl)methylamino]imidazo[4,5-c] quinolin-1-yl] butyl]carbamate (30 g, 53.41 mmol, 1 eq) was added to HCl (12M, 200 mL) at 25°C. The mixture was stirred at 25°C for 12 hour. LCMS showed the starting material was consumed completely. The reaction mixture was filtered, washed with MeOH (500 mL) and the filtrate was concentrated to give the crude product, recrystallized from EtOAc (50 mL) to give the pure 1-(4-aminobutyl)-2-butyl-imidazo[4,5-c]quinolin-4-amine (17 g, 48.38 mmol, 90.58% yield, 99% purity, HCl) as white solid. 1H NMR (MeOD, 400 MHz) δ 8.28 (d, J = 7.6 Hz, 1H), 7.82 (d, J = 8.4 Hz, 1H), 7.75 (t, J =7.6 Hz, 1H), 7.76 (t, J = 7.6 Hz, 1H), 4.72 (t, J = 7.6 Hz, 2H), 3.08 (t, J = 7.6 Hz, 2H), 3.01

(t, J = 7.6 Hz, 2H), 2.07-1.85 (m, 6H), 1.62-1.53 (m, 2H), 1.05 (t, J = 7.6 Hz, 3H). LCMS (ESI): $[M+H]^+$. calculated 312.21, $[M+H]^+$ found 312.

Supplemental Figure 1:

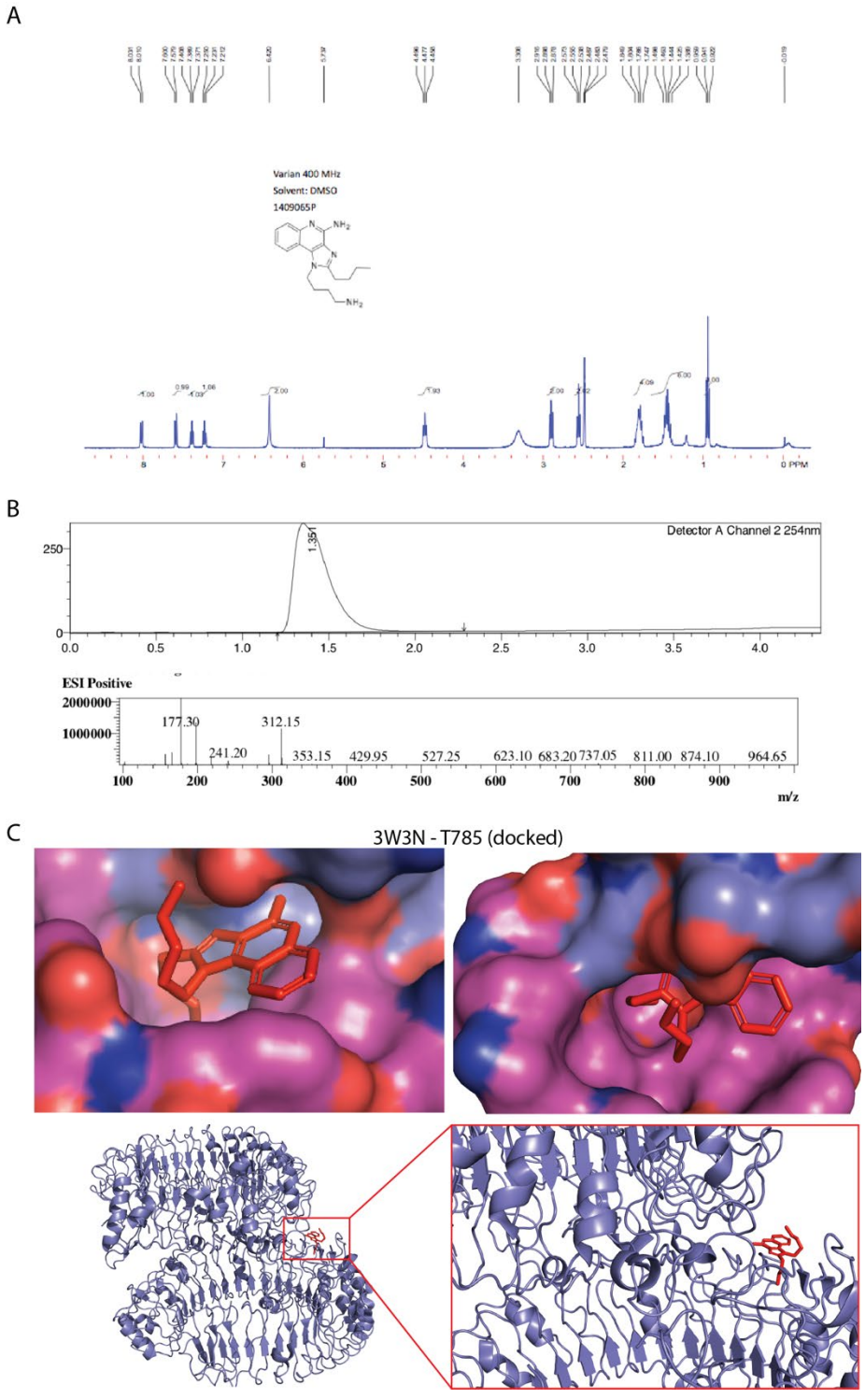

Supplemental Figure 1: T785 synthesis and design. (**A, B**) Confirmation of T785 structure via (**A**) proton NMR and (**B**) LC-MS. (**C**) Molecular docking studies using a co-crystal structure of human TLR8 and R848 (PDB ID: 3W3N) to visualize T785 in the binding pocket of TLR8 supported solvent accessibility of the point of conjugation. Zoomed in views of the binding pocket show solvent accessibility of the exit vector (upper panel) and a view of the entire TLR8 protein with a single T785 docked (lower panel).

Supplemental Figure 2:

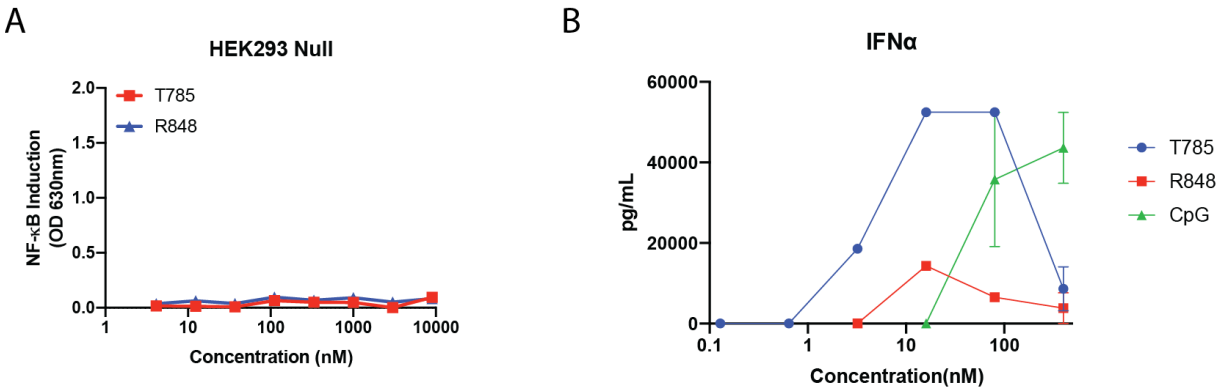

Supplemental Figure 2: T785 stimulation is TLR7/8 specific and elicits pDC activation. (A) HEK293 Null reporter cells, the parental cell line used for hTLR7 and hTLR8 reporter cells, were stimulated overnight with a concentration titration of T785 or R848 and activity was measured using QuantiBlue detection medium. (B) pDCs were isolated from healthy donor blood and stimulated overnight with T785 (TLR7/8), R848 (TLR7/8) or CpG (TLR9). Cytokine secretion was measured by ELISA.

Supplemental Figure 3:

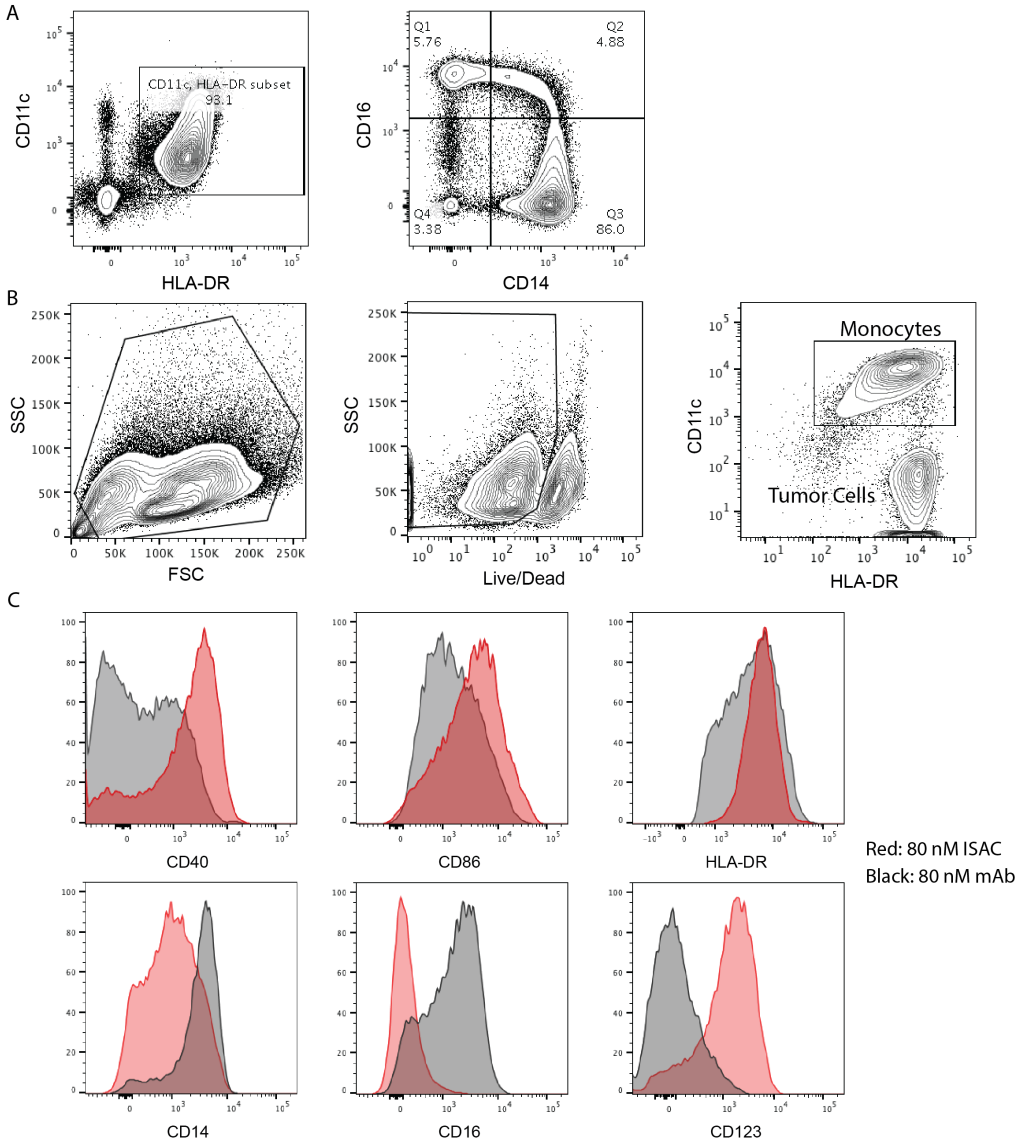

Supplemental Figure 3: Myeloid isolation and trastuzumab-ISAC activation. (**A**) Purity of freshly isolated myeloid APCs following negative selection by density gradient centrifugation using the RosetteSep Human Monocyte Enrichment Kit followed by magnetic separation with the EasySep Human Monocyte Enrichment Kit without CD16 Depletion as assessed by flow cytometry. **(B)** Gating strategy for analysis of activation and differentiation of myeloid APCs in all described in vitro experiments. First,

cells are gated as singlets by FSC or SSC to remove doublets. Next, a cellular size gate using SSC and FSC removes debris. Viable cells are then gated based on a Live/Dead stain. Finally, myeloid APCs are gated based on $CD11c^+$ and $HLA\text{-}DR^+$ expression. **(C)** Histogram analysis of cell surface marker expression of total myeloid APCs following stimulation with 80 nM rituximab-ISAC or 80 nM rituximab.

Supplemental Figure 4:

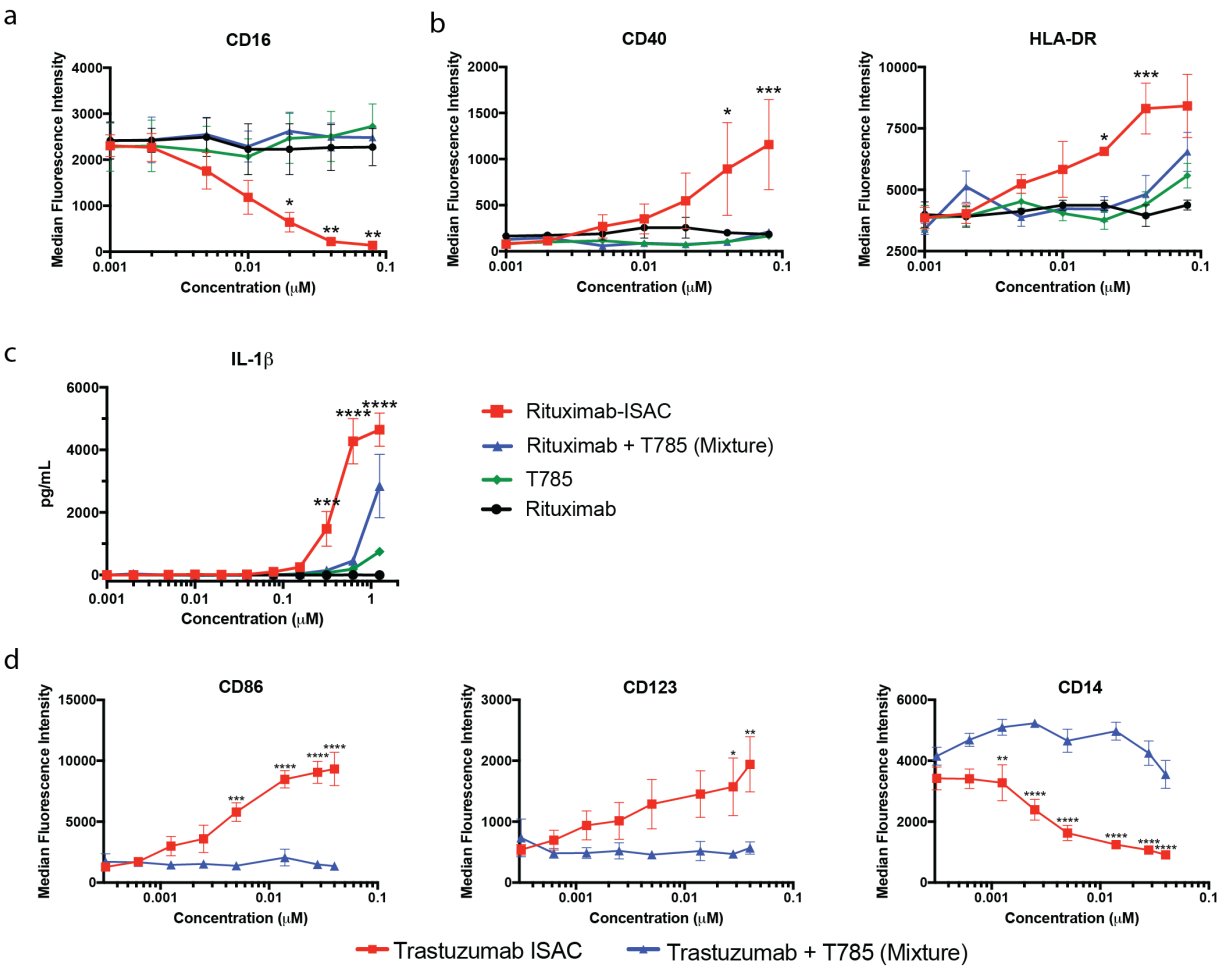

Supplemental Figure 4: Myeloid APC differentiation and activation following ISAC stimulation. Freshly isolated human myeloid APCs were cultured with rituximab, T785, rituximab and T785 or the rituximab T785-ISAC in the presence of CFSE-labeled $CD20^{+}$ Toledo tumor cells at a 3:1 ratio. The rituximab concentration is depicted on the X-axis with the concentration of T785 in these assays being consistent with the amount of T785 conjugated to the rituximab T785-ISAC. (**A-C**) Myeloid APCs were analyzed via flow cytometry or cytokine bead array 18 hours after stimulation. Data shown are from 3 donors and are representative of >10 donors (mean and SEM); *P<0.05, **P<0.01, ***P<0.001, ****P<0.0001. (**D**) Frozen myeloid APCs from were thawed, rested for two hours and incubated with trastuzumab or trastuzumab T785-ISAC for 18 hours prior to assessment of cell surface markers by FACS

analysis. Data are from 1 experiment and 3 donors and are representative of at least 3 experiments with 3 donors in each (shown as mean and SEM); *P<0.05, **P<0.01, ***P<0.001, ****P<0.0001.

Supplemental Figure 5:

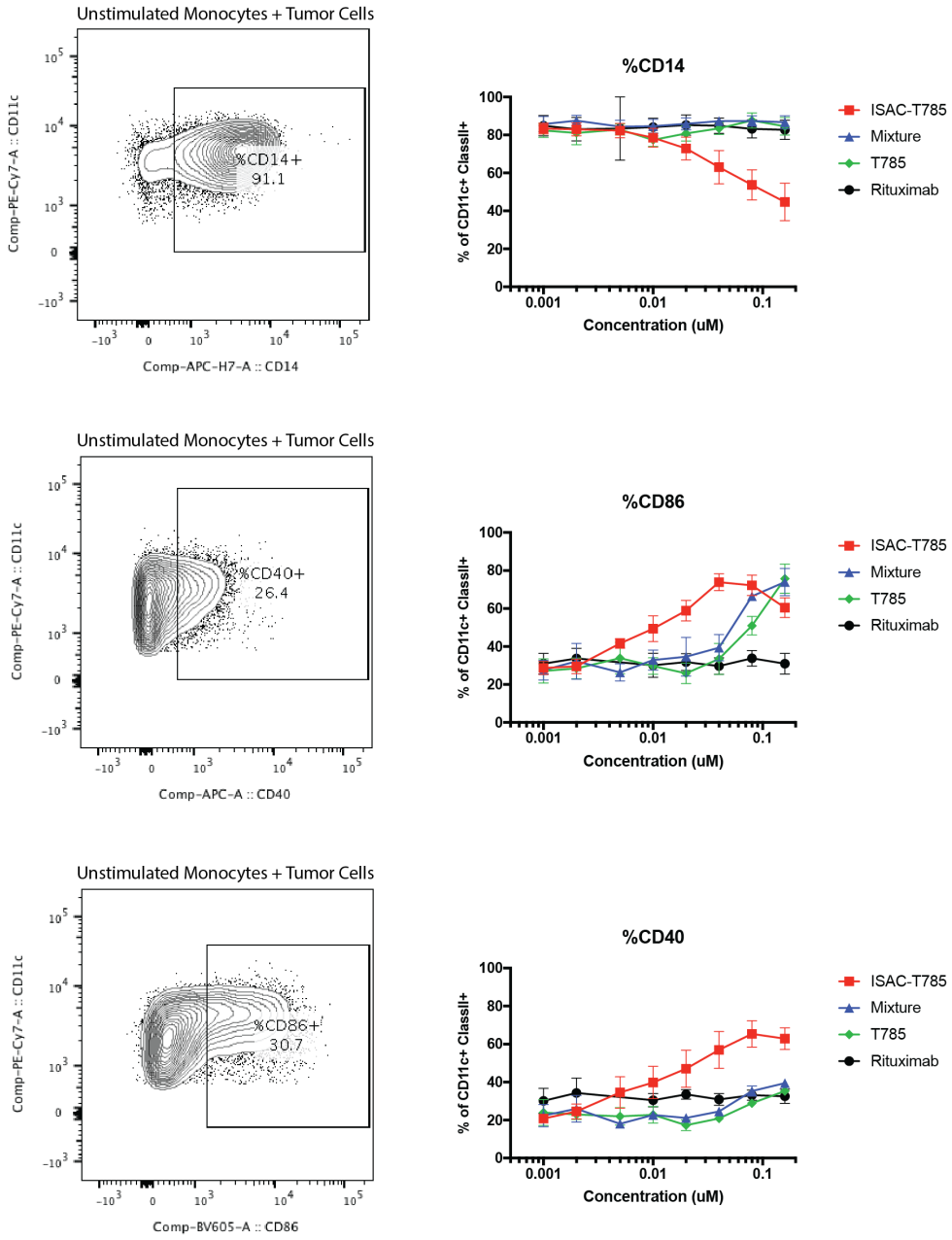

Supplemental Figure 5: Myeloid APC differentiation and activation following ISAC stimulation. The frequency of positive subsets (percentage positive) was calculated based on gating of unstimulated monocytes in the absence of tumor. On the left, the gating strategy is shown for unstimulated monocytes co-cultured with Toledo CD20^{+} tumor cells. A dose dependent response analogous to that measured with MFI (as reported in the manuscript) is observed when computed as percent positive of total monocytes.

Supplemental Figure 6:

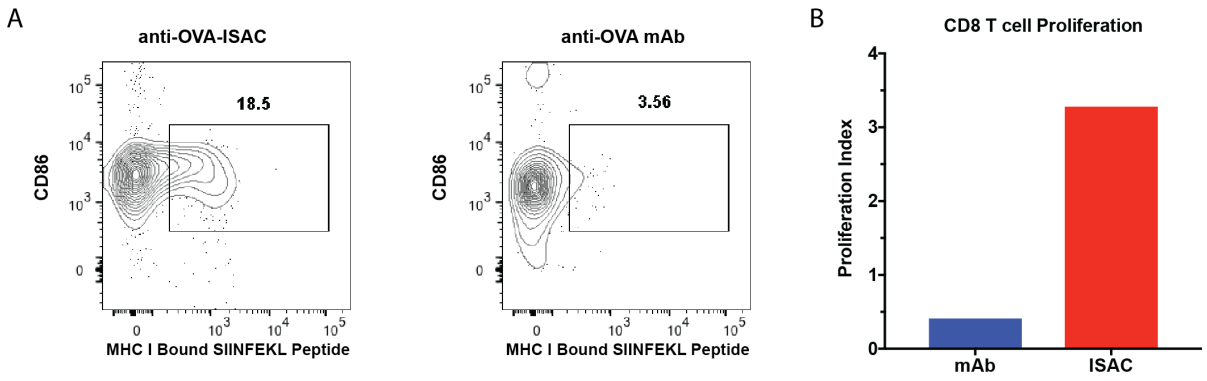

Supplemental Figure 6: ISAC stimulation leads to increased antigen cross-presentation and T cell proliferation. **(A)** Mouse splenocytes were isolated and cultured in vitro with ovalbumin antigen complexed with anti-OVA CL264-ISAC or anti-OVA mAb. Antigen cross-presentation was measured using multicolor flow cytometry through detection of MHC-I bound SIINFEKL peptide on total $CD11c^+$ splenic cells. **(B)** $CD8^+$ T cells with OVA-specific TCR were isolated from OT-1 transgenic mice and co-cultured with anti-OVA mAb or anti-OVA ISAC stimulated APCs. T cell proliferation was measured by final T cell count with the initial number of APCs substracted.

Supplemental Figure 7:

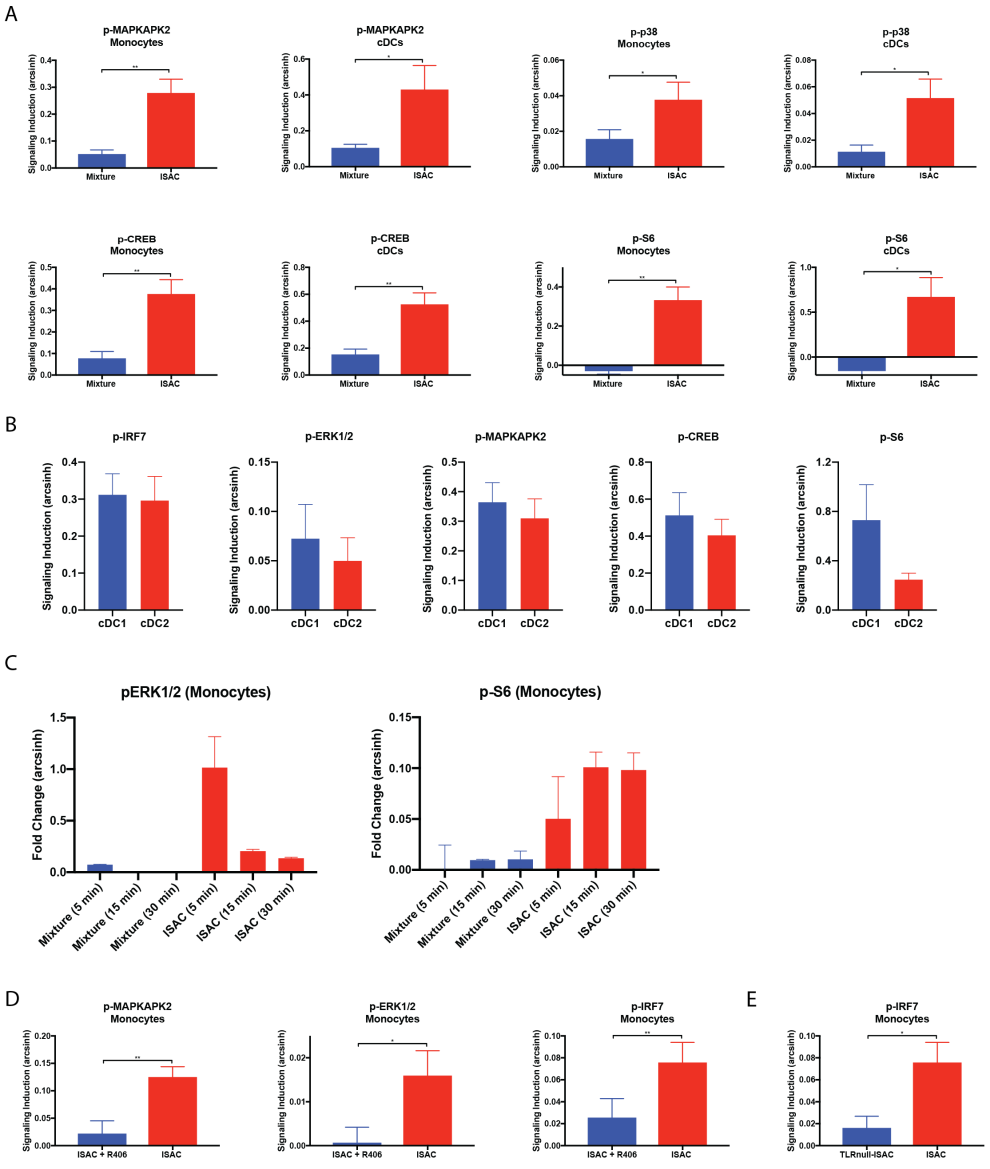

Supplemental Figure 7: ISACs elicit distinct intracellular signaling in monocytes and cDCs. (**A-E**) Freshly isolated human PBMC were stimulated 1 μM of rituximab-ISAC or an equimolar mixture of rituximab and T785 in the presence of $CD20^+$ Toledo tumor cells at a 1:1 ratio for 15 minutes. (**A**) Signaling induction of p-MAPKAPK2, p-p38, p-CREB and p-S6 in monocytes and cDCs was quantified by the arcsinh of the ISAC or mixture as compared to the unstimulated PBMCs. (**B**) cDCs

were subsetted as CD141 cDC1s and CD1c cDC2s. (**C**) Signaling through p-ERK1/2 and p-S6 measured following 5, 15, or 30-minute stimulation with rituximab T785-ISAC or the mixture of rituximab and T785. (**D**) Signaling induction of p-MAPKAPK2, p-ERK1/2 and p-IRF7 was quantified by the arcsinh of the ISAC with and without Syk blockade (R406) as compared to the unstimulated control. (**E**) Signaling induction of p-IRF7 was quantified by the arcsinh following stimulation with rituximab T785-ISAC or rituximab-TLRnull-ISAC (TLRnull-ISAC). (**A-E**) Data are from six donors (mean and SEM) for panels A, B, D, E and from two donors (mean and SEM) for panel C. Data are shown as mean with SEM; *P<0.05, **P<0.01, ***P<0.001, ****P<0.0001.

Supplemental Figure 8:

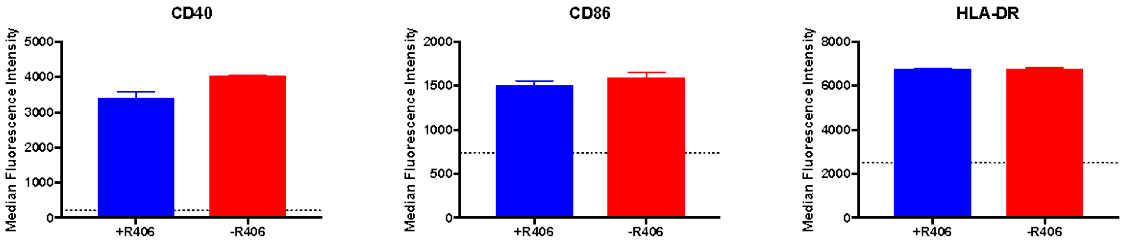

Figure 8: R406-mediated Syk inhibition does not alter T785 activity in human myeloid APCs. Monocytes were treated with 1 μM of R406 prior to stimulation with 2 μM T785 overnight. Activation was assessed by flow cytometry and no statistical significance was seen between the conditions with and without Syk inhibition. The dashed line represents the expression level of the unstimulated control.

Supplemental Figure 9:

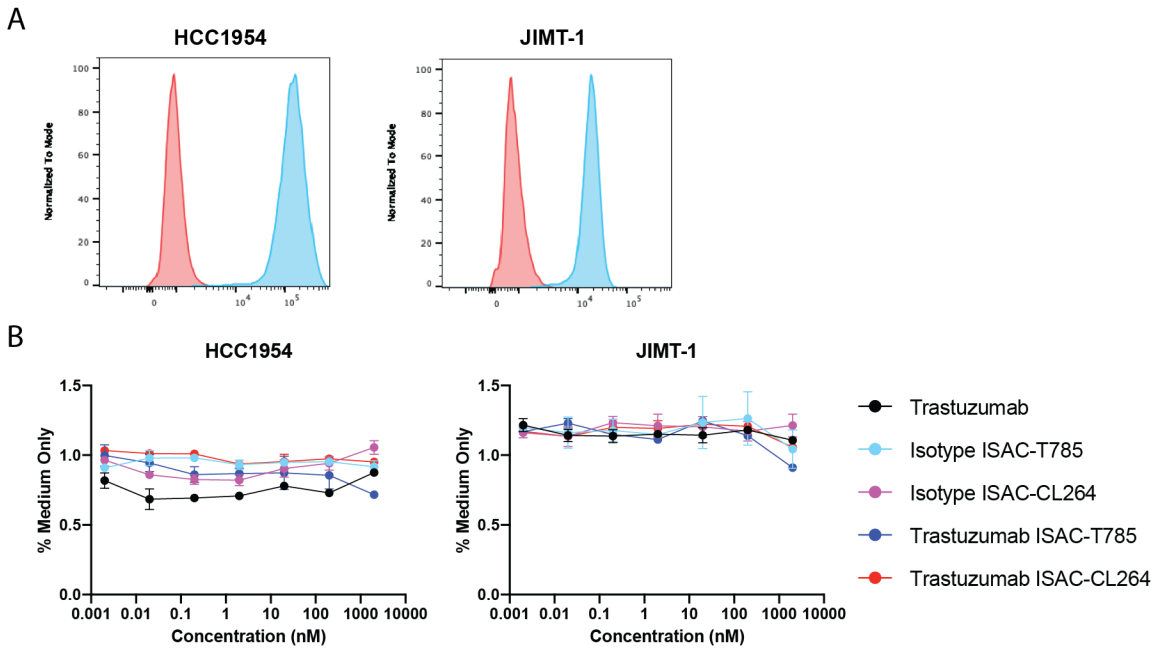

Supplemental Figure 9: In vitro cancer cell line proliferation with trastuzumab-ISACs. (**A**) In vitro HER2 expression by the indicated cancer cell lines as assessed by flow cytometry with PE-labeled anti-HER2 antibody (clone 24D2) (red) or the isotype control (blue). (**B**) Cancer cell line proliferation assayed with an MTT assay kit 72 hours after incubation with the indicated tumor cell line and the indicated test article. Rituximab-ISACs were utilized as isotype controls. Data are from 2 experiments performed in triplicate.

Supplemental Figure 10:

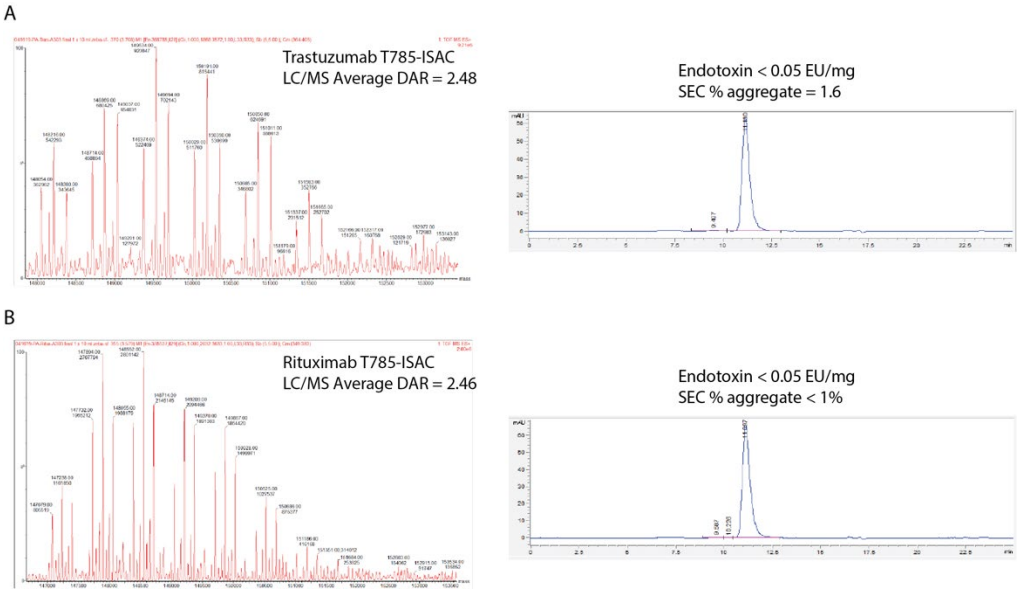

Supplemental Figure 10: Analytical data for representative trastuzumab and rituximab T785-ISACs. LC/MS and analytical SEC were performed to analyze ISACs following conjugation. For both the trastuzumab T785-ISAC (**A**) and rituximab T785-ISAC (**B**) had average DAR levels of 2.48 and 2.46, respectively. Conjugates were also found to be endotoxin low, with less than 0.05 EU/mg detected. Analytical SEC was performed to measure aggregation following conjugation, and both conjugates were found to have <2% aggregate present.

Supplemental Figure 11:

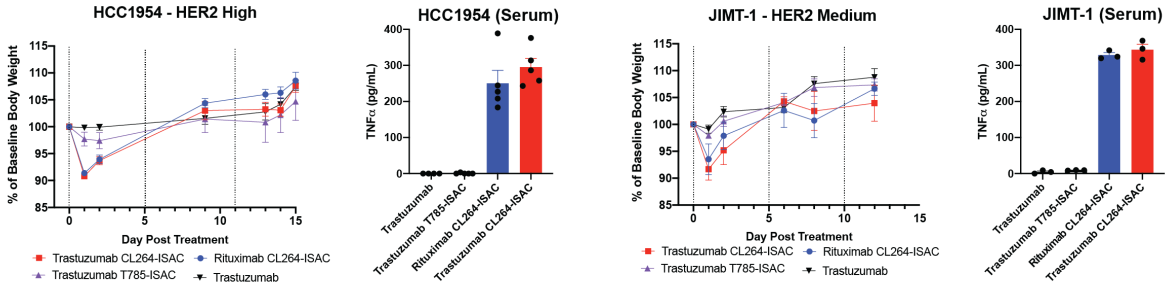

Supplemental Figure 11: T785-ISACs are well tolerated; CL264-ISACs lead to systemic cytokine secretion and transient body weight loss. NSG or Rag2/IL2rg double knockout mice were implanted with the indicated human tumor cell line and randomized when the tumor volume reached 50 – 75 mm^3 (HCC1954) or 75 – 150 mm^3 (JIMT-1). Mice were treated via intraperitoneal injection with 5 mg/kg of trastuzumab, trastuzumab T785-ISAC, trastuzumab CL264-ISAC or the respective isotype ISACs and cytokine secretion was measured by ELISA 4 hours following administration. Body weight was measured following dosing every 5 days, with doses indicated by dashed vertical lines.

Supplemental Figure 12:

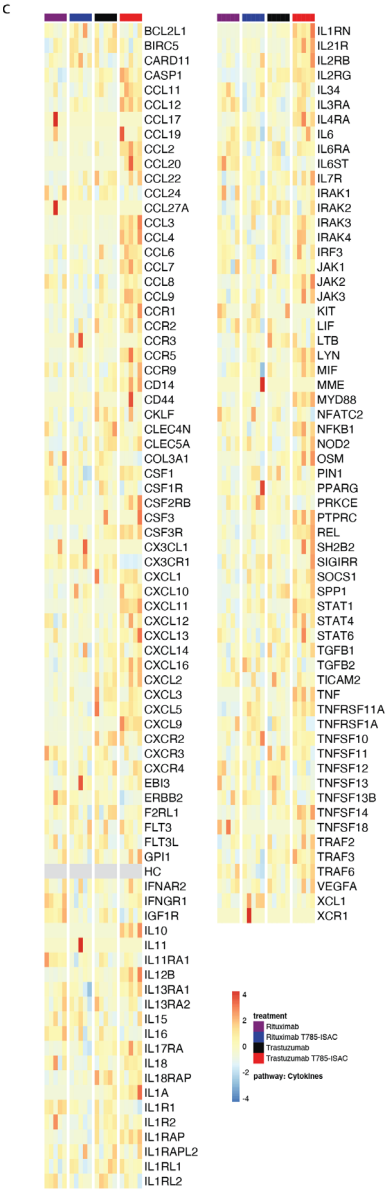

Supplemental Figure 12: Gene expression data for all genes used to calculate gene signatures in HCC1954 model. NanoString gene expression data was obtained using the mouse pan-cancer immune profiling panel, and gene expression pathway signature analysis was performed using the nSolver Advanced Analysis Pathway Score algorithm. Data are shown as heat maps for all genes used to calculate gene signature scores for (**A**) Dendritic Cell Functions, Macrophage Functions, Antigen Processing and Presentation, (**B**) Chemokines and (**C**) Cytokines.

Supplemental Figure 13:

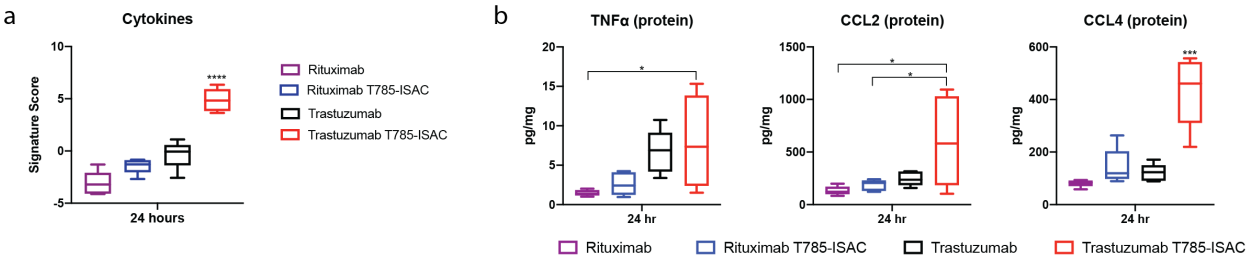

Supplemental Figure 13: Trastuzumab T785-ISAC treatment induces increased cytokine and chemokine secretion. HCC1954 tumors were implanted into SCID/Beige mice and were harvested from cohorts of mice 24 hours after a single dose of 5 mg/kg ISAC or control antibodies (n=5 mice per group). (**A**) Tumors were analyzed by NanoString mRNA quantification and data was analyzed by nSolver Advanced Analysis Pathway Scoring to measure changes in the Cytokines signature. (**B**) Cytokine secretion was measured in tumor lysates by MSD. Data are shown as mean with SEM and statistics are shown with *P<0.05, **P<0.01, ***P<0.001, ****P<0.0001.

Supplemental Figure 14:

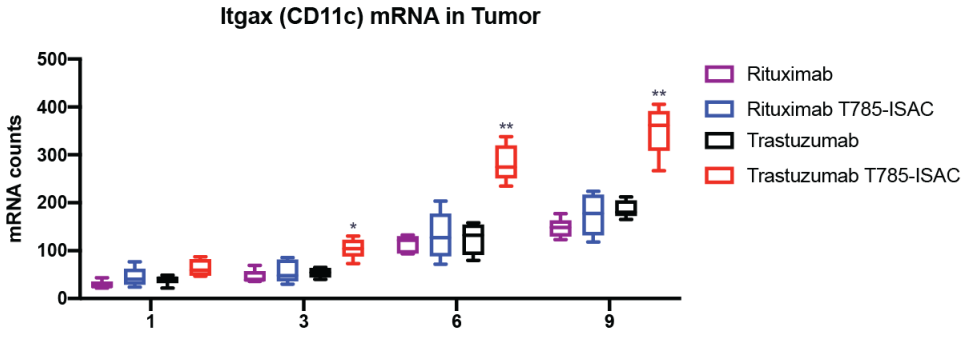

Supplemental Figure 14: Trastuzumab T785-ISAC treatment in HCC1954 xenograft model induces increased CD11c gene expression. HCC1954 tumors were implanted into SCID/Beige mice and were harvested from cohorts of mice 1, 3, 6, or 9 days after treatment with a single dose of 5 mg/kg ISAC or control antibodies (n=5 mice per group). Tumors were analyzed by NanoString mRNA quantification. Data are shown as mean with SEM and statistics are shown with *P<0.05, **P<0.01, ***P<0.001, ****P<0.0001.

Supplemental Figure 15:

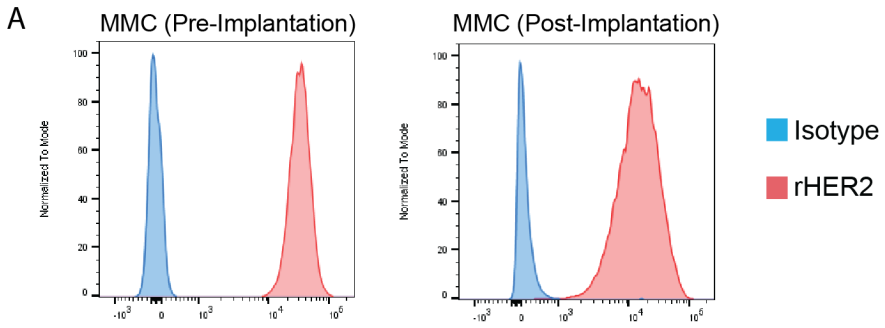

Supplemental Figure 15: rHER2 expression on MMC syngeneic tumor cell lines pre- and post-implantation. rHER2 expression was measured on the MMC tumor cell line by flow cytometry with fluorescently-conjugated anti-rHER2 antibody (red) or an isotype control (blue). For the MMC tumor cell line, antigen expression was assessed 23 days post implantation.

Supplemental Figure 16:

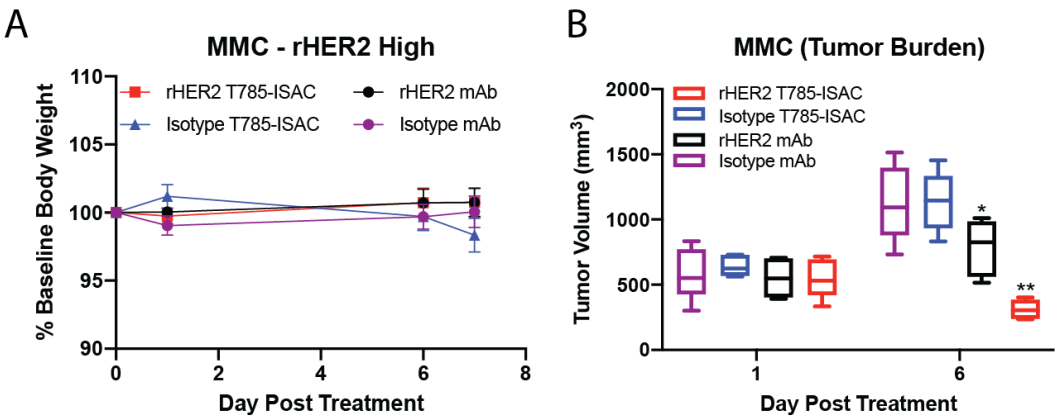

Supplemental Figure 16: Body weight and tumor burden following rHER2 T785-ISAC treatment in MMC tumor model. (**A**) Treatment with rHER2 T785 ISAC or its controls led to no measurable significant impact on body weight relative to the baseline body weight measured prior to initiation of treatment. (**B**) MMC tumor burden was measured at 1 and 6 days post initiation of treatment with 5 mg/kg rHER2 T785-ISAC or its controls. Tumors were measured and then harvested at each time point for further analysis by NanoString, MSD protein quantification, and immunohistochemistry. Data are shown as mean with SEM; *P<0.05, **P<0.01, ***P<0.001, ****P<0.0001.

Supplemental Figure 17:

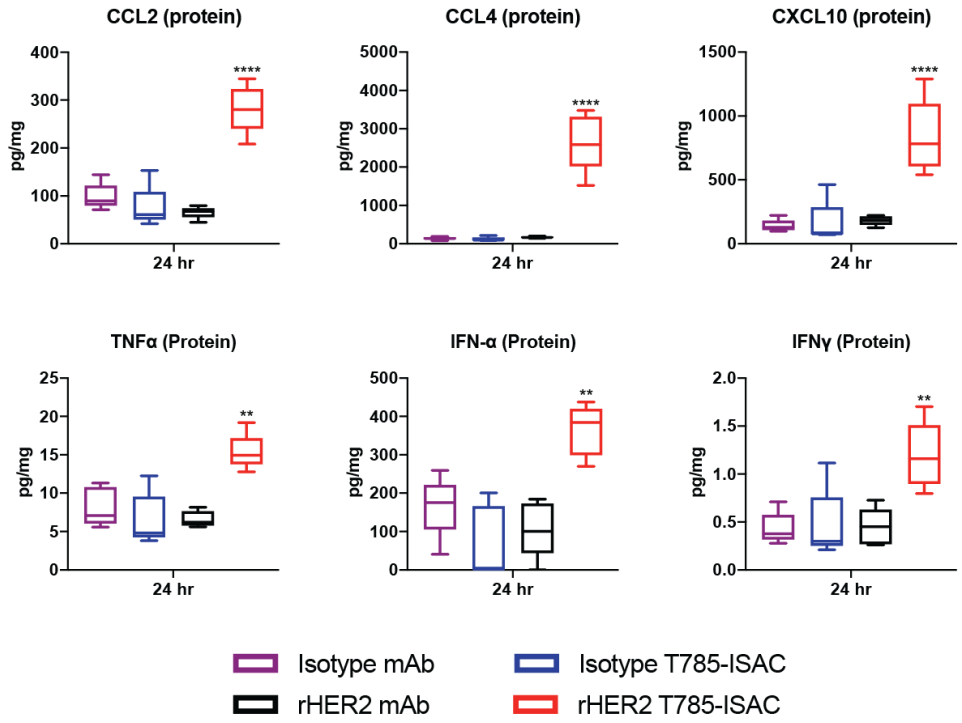

Supplemental Figure 17: rHER2 T785-ISAC treatment in the MMC model triggers chemokine and pro-inflammatory cytokine production in the tumor. MMC tumor cells were implanted in FVB/N-TgN (MMTV-Erbb2) mice. Mice were treated via intraperitoneal injection with 5 mg/kg of mouse anti-rat HER2 antibody, mouse anti-rat HER2 T785-ISAC or their respective isotype controls upon reaching a tumor volume of about 500 mm^3. Cytokine levels were measured in tumor lysates 24 hours after administration by MSD. Data are shown as mean with SEM; *P<0.05, **P<0.01, ***P<0.001, ****P<0.0001.

Supplemental Figure 18:

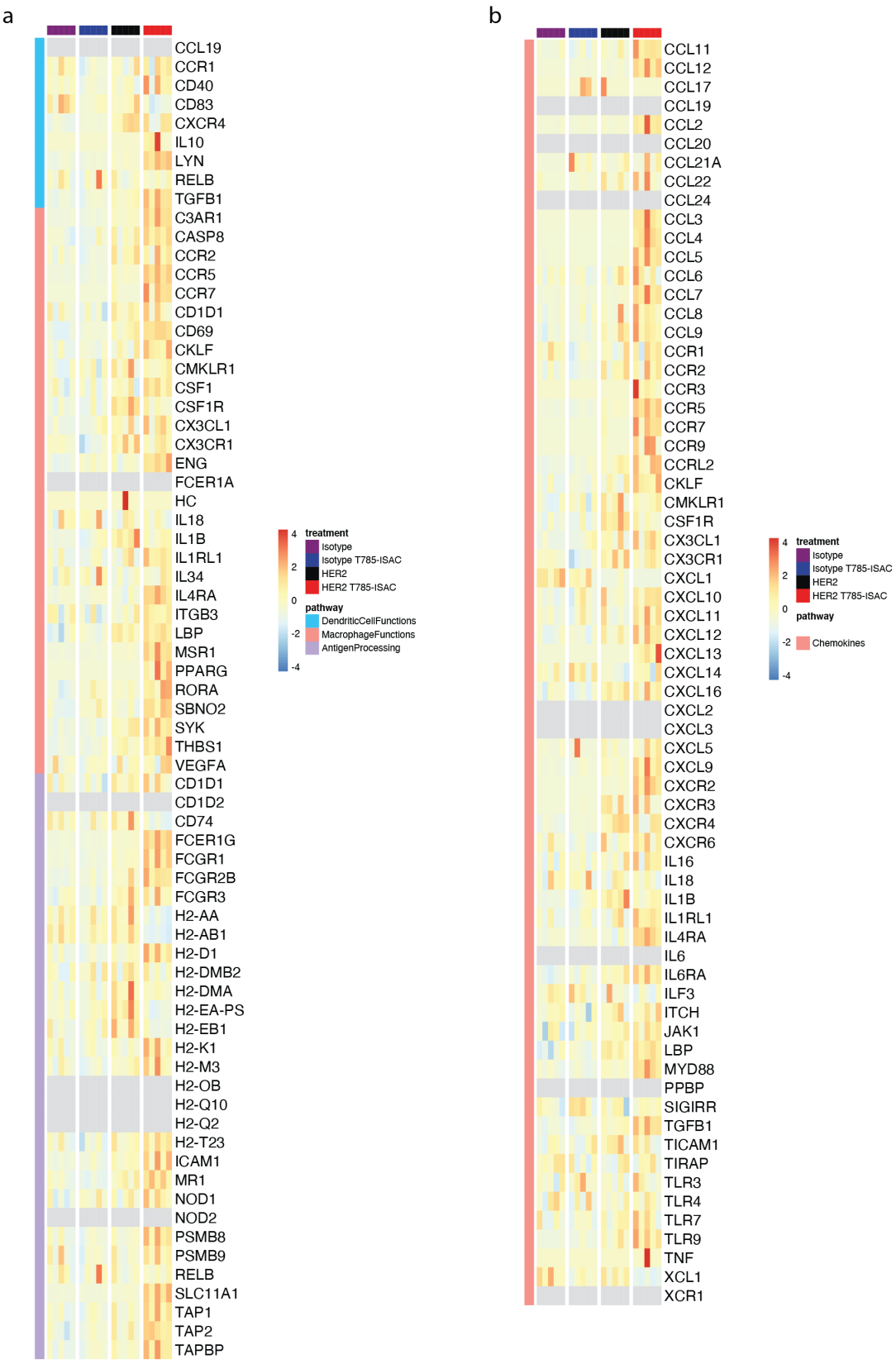

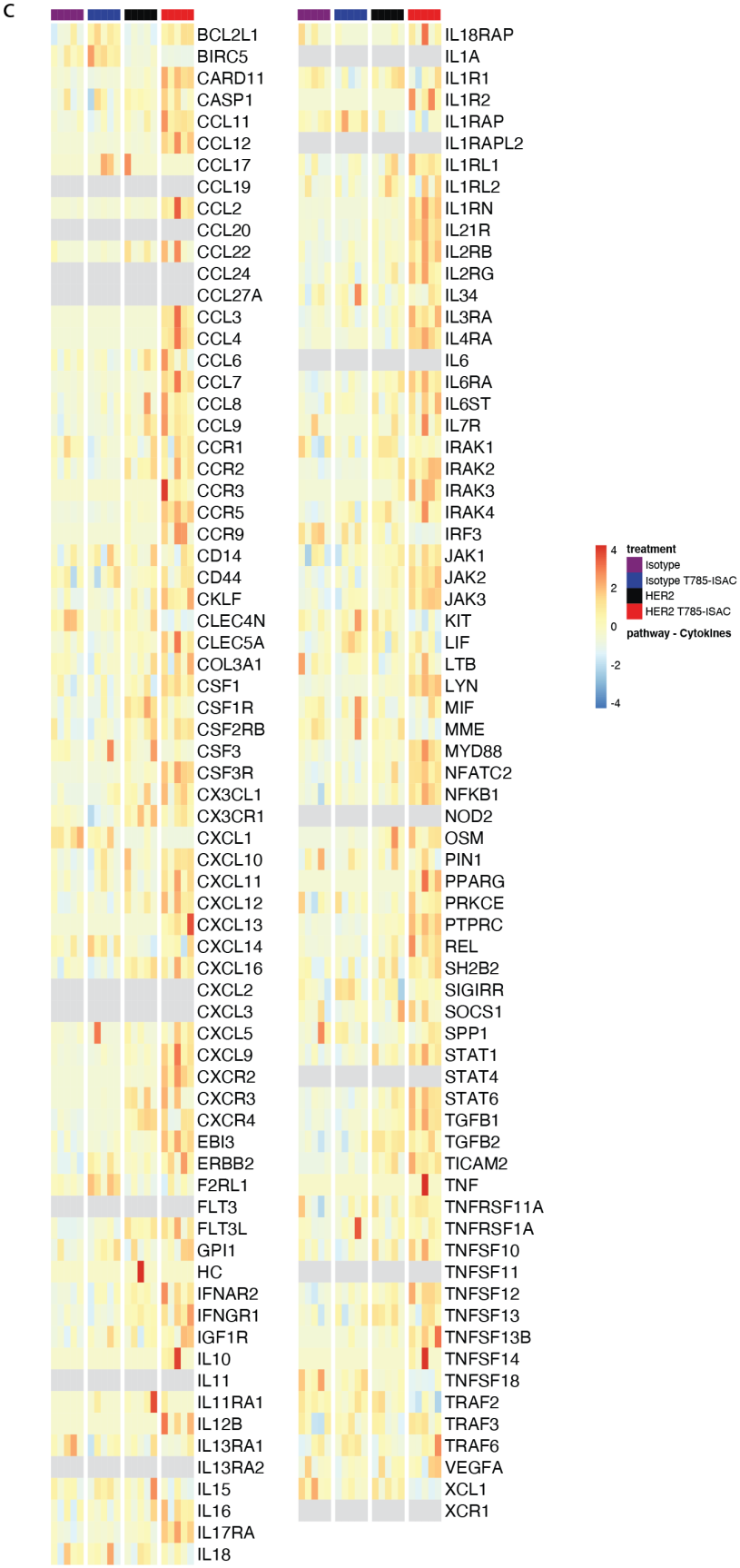
C
BCL2L1
BIRC5
CARD11
CASP1
CCL11
CCL12
CCL17
CCL19
CCL2
CCL20
CCL22
CCL24
CCL27A
CCL3
CCL4
CCL6
CCL7
CCL8
CCL9
CCR1
CCR2
CCR3
CCR5
CCR9
CD14
CD44
CKLF
CLEC4N
CLEC5A
COL3A1
CSF1
CSF1R
CSF2RB
CSF3
CSF3R
CX3CL1
CX3CR1
CXCL1
CXCL10
CXCL11
CXCL12
CXCL13
CXCL14
CXCL16
CXCL2
CXCL3
CXCL5
CXCL9
CXCR2
CXCR3
CXCR4
EBI3
ERBB2
F2RL1
FLT3
FLT3L
GPI1
HC
IFNAR2
IFNGR1
IGF1R
IL10
IL11
IL11RA1
IL12B
IL13RA1
IL13RA2
IL15
IL16
IL17RA
IL18
IL18RAP
IL1A
IL1R1
IL1R2
IL1RAP
IL1RAPL2
IL1RL1
IL1RL2
IL1RN
IL21R
IL2RB
IL2RG
IL34
IL3RA
IL4RA
IL6
IL6RA
IL6ST
IL7R
IRAK1
IRAK2
IRAK3
IRAK4
IRF3
JAK1
JAK2
JAK3
KIT
LIF
LTB
LYN
MIF
MME
MYD88
NFATC2
NFKB1
NOD2
OSM
PIN1
PPARG
PRKCE
PTPRC
REL
SH2B2
SIGIRR
SOCS1
SPP1
STAT1
STAT4
STAT6
TGFB1
TGFB2
TICAM2
TNF
TNFRSF11A
TNFRSF1A
TNFSF10
TNFSF11
TNFSF12
TNFSF13
TNFSF13B
TNFSF14
TNFSF18
TRAF2
TRAF3
TRAF6
VEGFA
XCL1
XCR1
4
2
0
-2
-4
treatment
Isotype
Isotype T785-ISAC
HER2
HER2 T785-ISAC
pathway - Cytokines

d

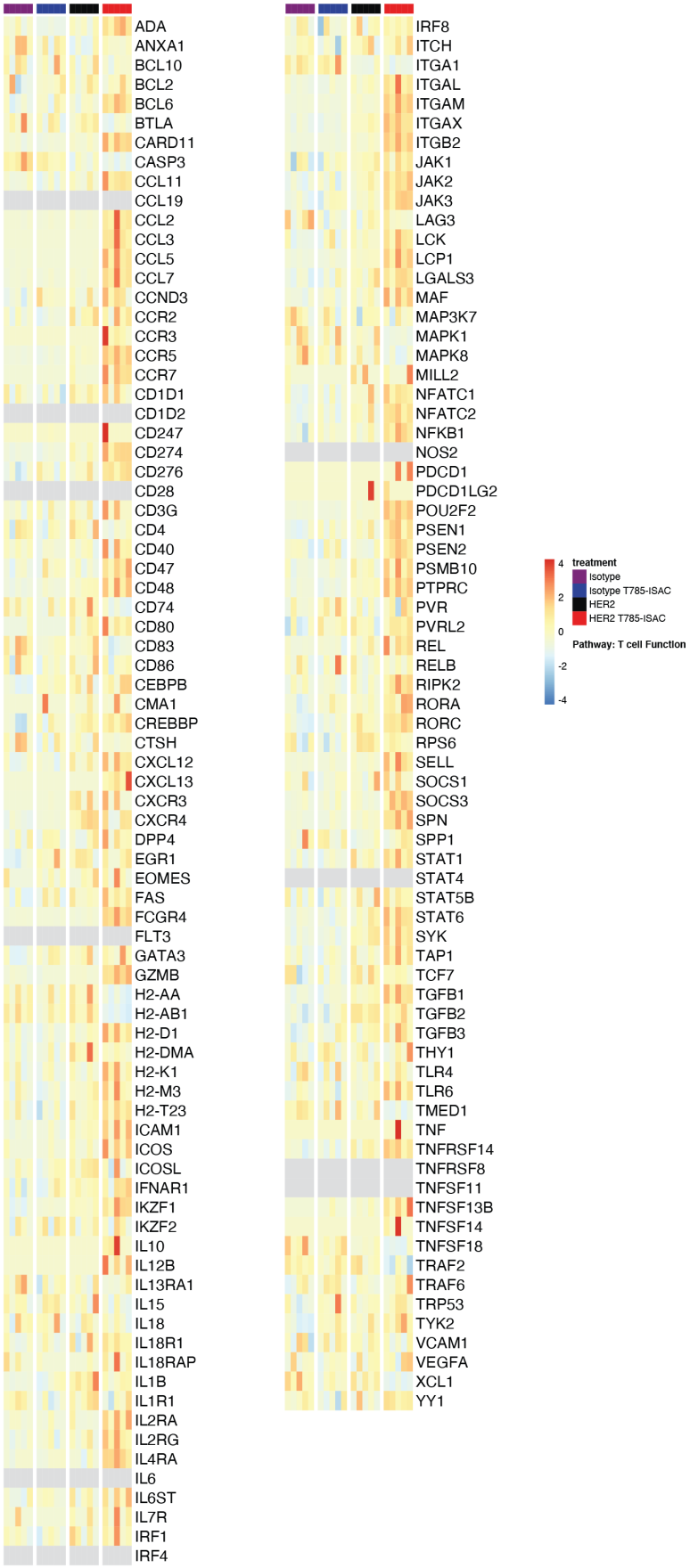
ADA
ANXA1
BCL10
BCL2
BCL6
BTLA
CARD11
CASP3
CCL11
CCL19
CCL2
CCL3
CCL5
CCL7
CCND3
CCR2
CCR3
CCR5
CCR7
CD1D1
CD1D2
CD247
CD274
CD276
CD28
CD3G
CD4
CD40
CD47
CD48
CD74
CD80
CD83
CD86
CEBPB
CMA1
CREBBP
CTSH
CXCL12
CXCL13
CXCR3
CXCR4
DPP4
EGR1
EOMES
FAS
FCGR4
FLT3
GATA3
GZMB
H2-AA
H2-AB1
H2-D1
H2-DMA
H2-K1
H2-M3
H2-T23
ICAM1
ICOS
ICOSL
IFNAR1
IKZF1
IKZF2
IL10
IL12B
IL13RA1
IL15
IL18
IL18R1
IL18RAP
IL1B
IL1R1
IL2RA
IL2RG
IL4RA
IL6
IL6ST
IL7R
IRF1
IRF4
IRF8
ITCH
ITGA1
ITGAL
ITGAM
ITGAX
ITGB2
JAK1
JAK2
JAK3
LAG3
LCK
LCP1
LGALS3
MAF
MAP3K7
MAPK1
MAPK8
MILL2
NFATC1
NFATC2
NFKB1
NOS2
PDCD1
PDCD1LG2
POU2F2
PSEN1
PSEN2
PSMB10
PTPRC
PVR
PVRL2
REL
RELB
RIPK2
RORA
RORC
RPS6
SELL
SOCS1
SOCS3
SPN
SPP1
STAT1
STAT4
STAT5B
STAT6
SYK
TAP1
TCF7
TGFB1
TGFB2
TGFB3
THY1
TLR4
TLR6
TMED1
TNF
TNFRSF14
TNFRSF8
TNFSF11
TNFSF13B
TNFSF14
TNFSF18
TRAF2
TRAF6
TRP53
TYK2
VCAM1
VEGFA
XCL1
YY1
4
2
0
-2
-4
treatment
Isotype
Isotype T785-ISAC
HER2
HER2 T785-ISAC
Pathway: T cell Function

Supplemental Figure 18: Gene expression data for all genes used to calculate gene signatures in MMC model. NanoString gene expression data was obtained using the mouse pan-cancer immune profiling panel, and gene expression pathway signature analysis was performed using the nSolver Advanced Analysis Pathway Score algorithm. Data are shown as heat maps for all genes used to calculate gene signature scores for (**A**) Dendritic Cell Functions, Macrophage Functions, Antigen Processing and Presentation, (**B**) Chemokines, (**C**) Cytokines, and (**D**) T Cell Functions.

Supplemental Figure 19:

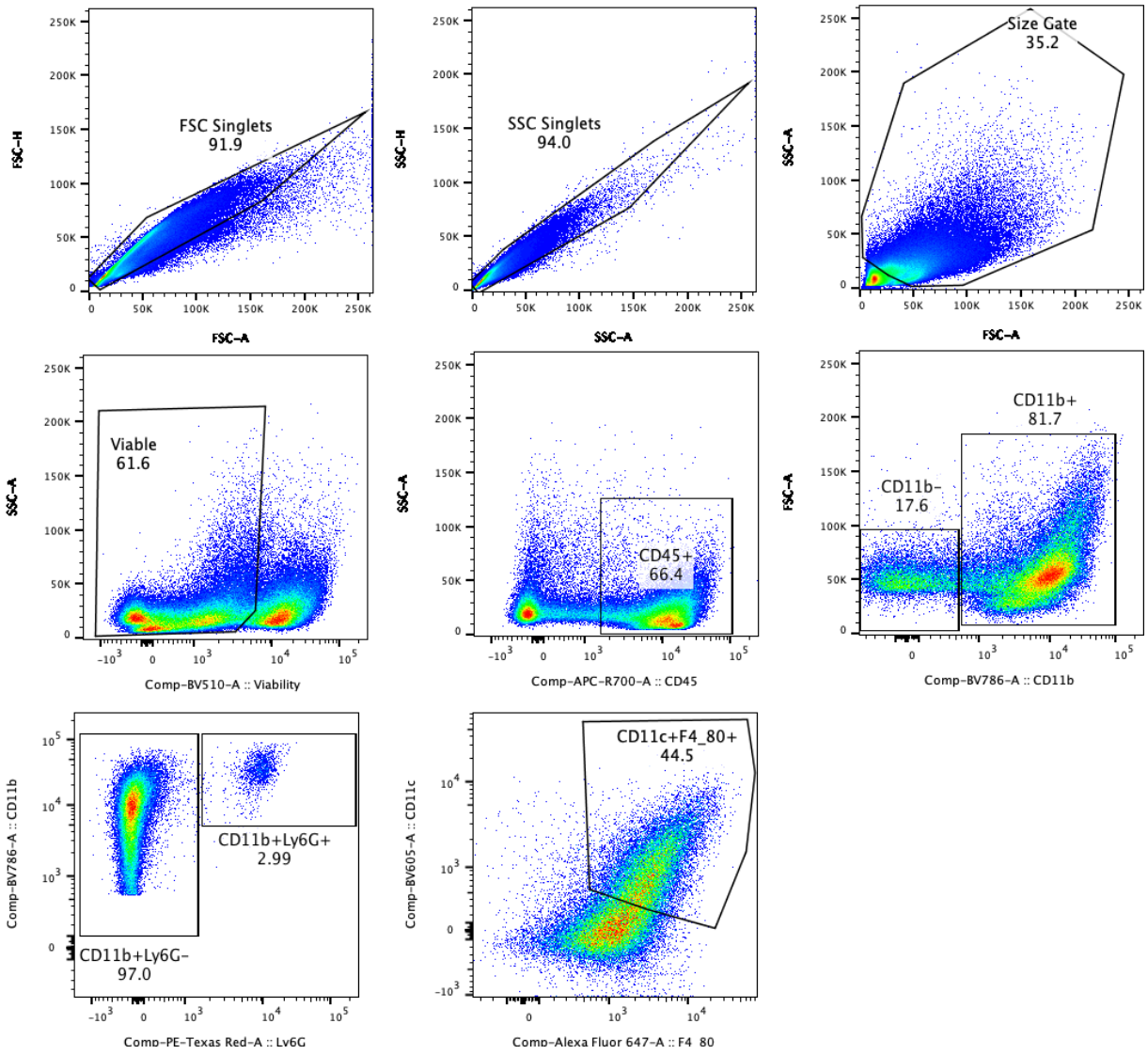

Supplemental Figure 19: Gating scheme for flow cytometry analysis of tumor samples from MMC syngeneic tumor model. Myeloid APCs are defined as viable cells with CD45+Ly6G-CD11b+CD11c+F4/80+ expression.

Supplemental Figure 20:

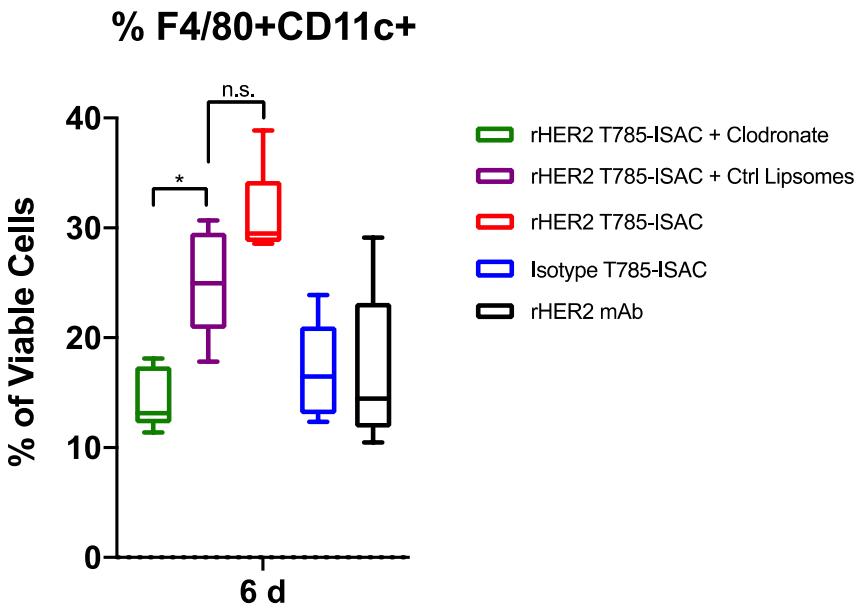

Supplemental Figure 20: Phagocyte depletion in the MMC model leads to absence of myeloid APC increase seen following ISAC treatment. FVB/N-TgN (MMTV-Erbb2) mice were implanted with the MMC tumor cell line. Mice were randomized the tumor volume reached about 500 mm^3 and were pre-treated with clodronate-loaded or control liposomes for phagocyte depletion. Animals were then treated with 5 mg/kg rHER2 T785-ISAC mouse anti-rat HER2 antibody, mouse anti-rat HER2 T785-ISAC, or isotype T785-ISAC (TA99) given twice every 5 days (n=5 mice per arm). Tumors were harvested 6 days following initiation of treatment and were analyzed by flow cytometry, with myeloid APCs defined as viable cells with CD45+CD11b+CD11c+F4/80+ expression. Data are shown as mean with SEM; *P<0.05, **P<0.01, ***P<0.001, ****P<0.0001.

Supplemental Figure 21:

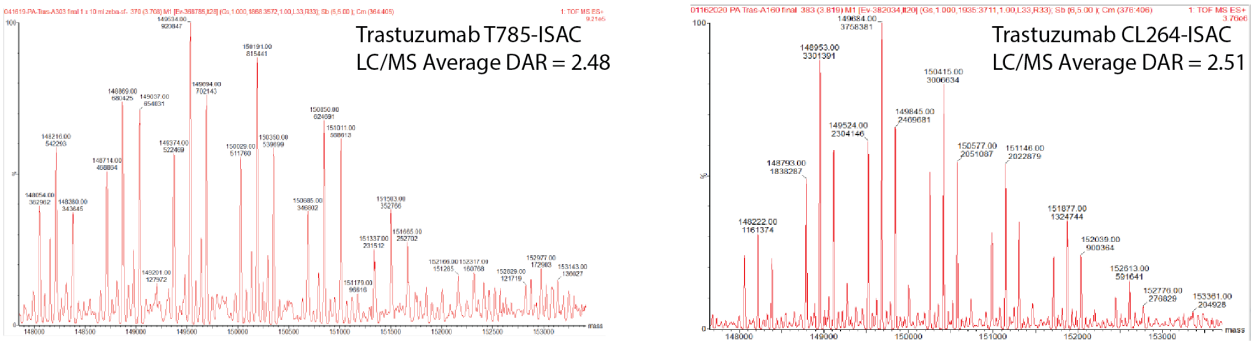

Supplemental Figure 21: Analytical data for representative trastuzumab T785-ISAC and CL264-ISAC. LC/MS and analytical SEC were performed to analyze ISACs following conjugation. The trastuzumab T785-ISAC had an average DAR level of 2.48 while the trastuzumab CL264-ISAC had an average DAR of 2.51. Conjugates were also found to be endotoxin low, with less than 0.05 EU/mg detected.

Supplemental Figure 22:

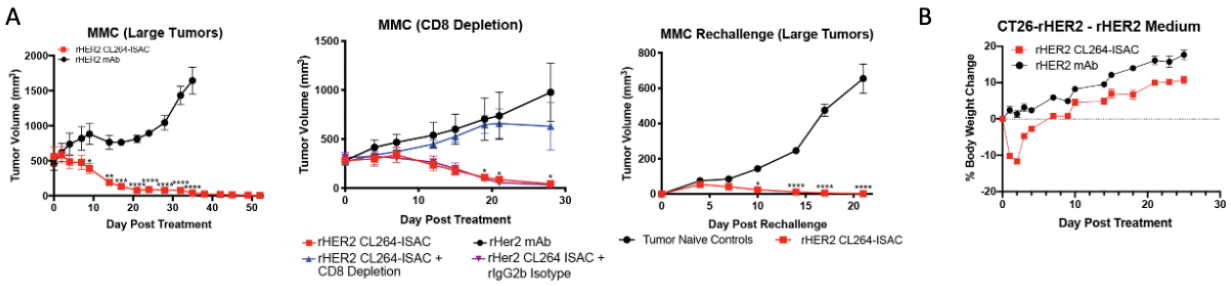

Supplemental Figure 22: CL264-ISACs lead to systemic cytokine secretion and transient body weight loss; T-cell dependent efficacy in MMC syngeneic tumor model. (**A**) FVB/N-TgN (MMTV-Erbb2) mice were implanted with the MMC tumor cell line. Mice were randomized when the average tumor volume reached 500 mm^3 and treated via intraperitoneal injection with 5 mg/kg of mouse anti-rat HER2 antibody or mouse anti-rat HER2 CL264-ISAC every 5 days for a total of 3 treatments (n=4 mice per arm). For CD8 T cell depletion, mice were randomized when the tumor volume reached ~280 mm^3. Mice were treated with an antibody to deplete CD8 T cells or with a rIgG2b control, and then treated via intraperitoneal injection with 2 mg/kg of mouse anti-rat HER2 antibody or mouse anti-rat HER2 CL264-ISAC every 7 days for a total of 2 treatments (n=5-7 mice per arm). Anti-rat HER2 CL264-ISAC treated mice that experienced complete tumor regression for >90 days (n=4 mice per arm) were challenged with the MMC tumor cell line. (**B**) Balb/c mice were implanted with the CT26-rHER2 tumor cell line and were randomized when the tumor volume reached 50 mm^3. Mice were then treated via intraperitoneal injection with 10 mg/kg of mouse anti-rat HER2 or mouse anti-rat HER2 CL264-ISAC every 5 days for a total of 6 treatments and body weight was measured relative to the baseline body weight prior to initiation of treatment. Data are shown as mean with SEM; *P<0.05, **P<0.01, ***P<0.001, ****P<0.0001.

Supplemental Figure 23:

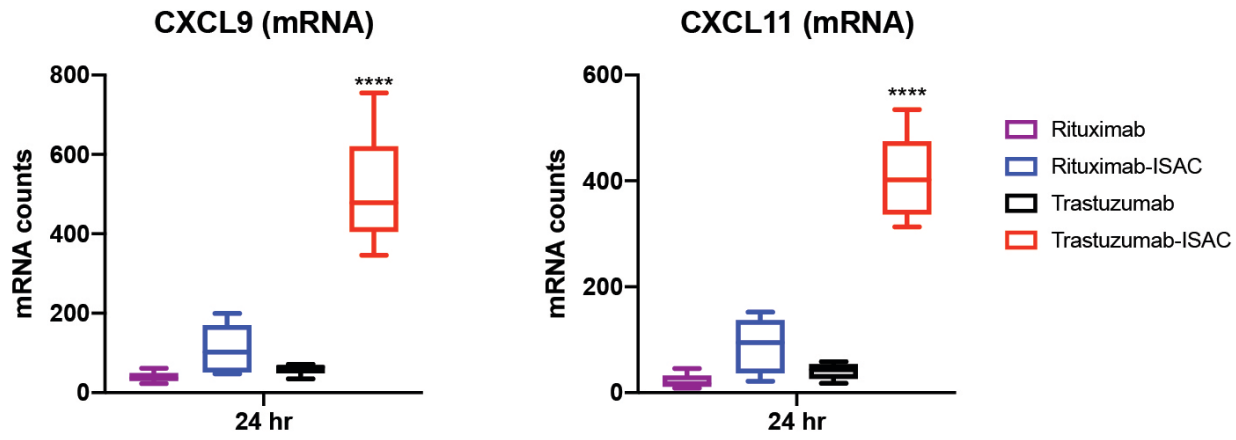

Supplemental Figure 23: ISACs elicit production of CXCL9 and CXCL11 in HCC1954 xenograft model. SCID/Beige mice were implanted with the human breast cancer cell line HCC1954. Mice were dosed with a single treatment of 5 mg/kg of trastuzumab, trastuzumab T785-ISAC, rituximab, or rituximab T785-ISAC by intraperitoneal injection. Tumors were harvested 24 hours after treatment and analyzed by Nanostring mRNA quantification. Data are from one experiment with 5 mice per group (mean and SEM); *P<0.05, **P<0.01, ***P<0.001, ****P<0.0001.

Supplemental Figure 24:

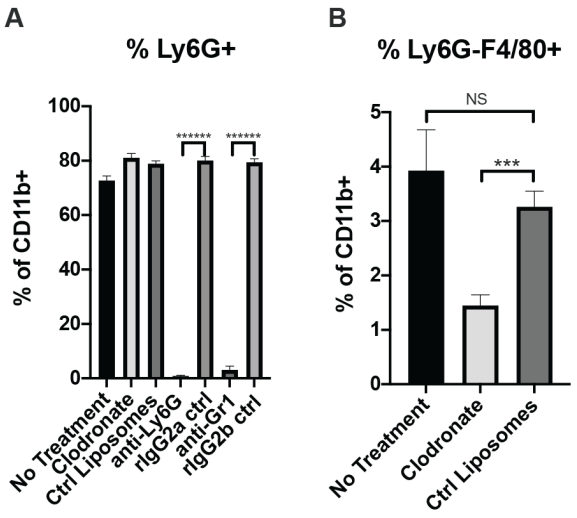

Supplemental Figure 24: Cell depletion is measured in the periphery following depleting treatments in the HCC1954 model. HCC1954 tumor cells were implanted into SCID/Beige mice, and cells of interest were depleted prior to and during trastuzumab T785-ISAC treatment using anti-Ly6G antibody (rat IgG2a control), clodronate liposomes (control liposomes) or anti-Gr1 antibody (rat IgG2b control). Data are from one experiment with n=4-6 mice per group and cells were analyzed by flow cytometry 13 days following initiation of treatment. (A) Percent of Ly6G+ cells of CD11b+ cells in blood taken during xenograft depletion study. (B) Percent of Ly6G-F4/80+ cells of CD11b+ cells in blood. Data are presented as mean with SEM; ******P<0.000001 and ***P <0.001.

Supplemental Table 1:

Fc Receptor Binding	Rituximab K_D (nM)	Rituximab-ISAC K_D (nM)
FCGR1 (CD64)	5.51 ± 0.298	5.08 ± 0.266
FCGR2A (CD32A)	4100 ± 196	3600 ± 253
FCGR2B (CD32B)	6230 ± 134	4790 ± 839
FCGR3A (CD16A)	377 ± 5.28	214 ± 9.16

Supplemental Table 1: Binding affinities of monoclonal antibody Rituximab and Rituximab-ISAC for the Fc gamma receptors. Rituximab or Rituximab T785-ISAC were injected over CM5 chips containing immobilized Fc gamma receptor proteins. Kinetics for FCGR1 and FCGR3A were analyzed using Biacore T200 evaluation software (V3.1) using kinetic fit (1:1). For low affinity receptors (FCGR2A and FCGR2B), KDs were determined using steady state affinity (1:1).

Supplemental Table 2:

Antibody	Element	Mass
CD32	La	139
CD3 (UCHT1)	Ce	140
p-PLCG2 (K86-689.37)	Pr	141
CD19 (HIB19)	Nd	142
CD123 (6H6)	Nd	143
p-Src (K98-37)	Nd	144
CD4 (RPA-T4)	Nd	145
CD8a (RPA-T8)	Nd	146
CD11c (Bu15)	Sm	147
CD64 (10.1)	Sm	148
p-STAT5 (Y694) (47)	Nd	150
CD107a	Eu	151
p-AKT	Sm	152
p-MAPKAPK (27B7)	Eu	153
p-SHP2 (pY580) (Polyclonal)	Sm	154
CD11b (ICRF44)	Gd	155
p-SLP76 (Y128) (J141-668.36.58)	Gd	156
CD1c	Gd	157
CD33	Gd	158
IRF7-PE-antiPE	Tb	159
p-ZAP70/Syk (Y319/Y352) (17a)	Gd	160
CD14 (M5E2)	Dy	161
p-CREB (S133) (87G3)	Dy	162
p-NFkB (S529) (K10-895.12.50)	Dy	163
p-PI3K	Dy	164
CD16	Ho	165
IkB (total) (L35A5)	Er	166
p-PLCG1 (Y783)	Er	167
p-ERK1/2 (20A)	Er	168
p-p38 (T180/Y182) (36/ p38)	Tm	169
CD40 (5C3)	Er	170
p-Btk/Itk (Y551/Y511) (24a/BTK)	Yb	171
p-S6 (S235/S236) (N7-548)	Yb	172
p-STAT3 (Y705) (4)	Yb	173
p-Jnk/SAPK (T183/Y185) (G9)	Yb	174
CD141	Lu	175
CD56 (NCAM16.2)	Yb	176
DNA1	Ir	191
DNA2	Ir	193
HLA-DR	Bi	209

Supplemental Table 2: CyTOF antibody panel for the assessment of intracellular signaling in human PBMCs. A panel of antibodies targeting surface and intracellular markers was designed to enable phenotyping and sub-setting of immune cells found within PBMCs as well as measure signaling across diverse signaling pathways.